

Supplementary Materials: Coupled Stratospheric Chemistry-Meteorology Data Assimilation. Part I: Modeling chemistry-dynamics interactions

Richard Ménard^{1,†,*}, Simon Chabrillat^{2,‡}, Alain Robichaud¹, Jean de Grandpré¹, Martin Charron³, Yves Rochon¹, Rebecca Batchelor⁴, Alexander Kallaur¹, Mateusz Reszka⁵ and Jacek Kaminski⁶

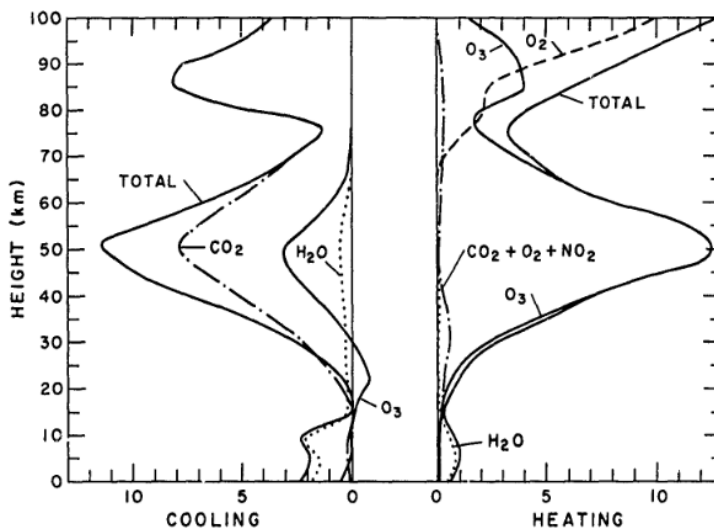


Figure S1. Vertical distribution of solar short wave heating rates and long wave cooling rates (in °K/day) (from London 1980)

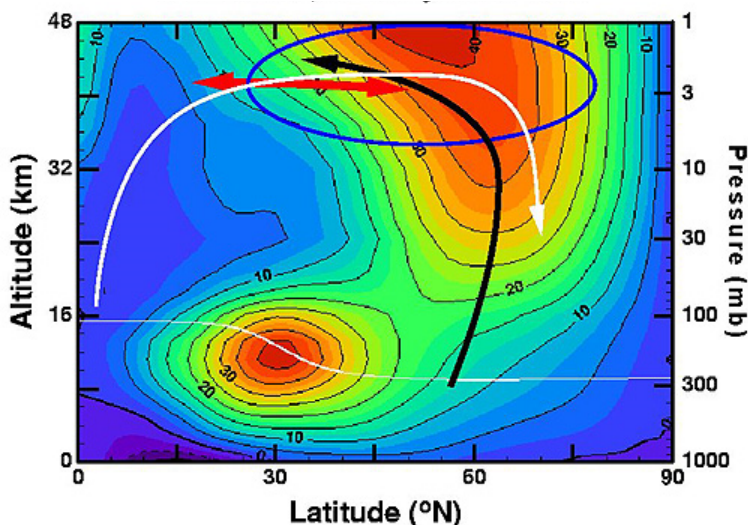


Figure S2. Schematic of the Brewer-Dobson circulation Northern hemisphere winter (Courtesy NASA Studying Earth's Environment from Space). Color contours of zonal wind (m/s). Black arrow shows the path of vertically propagating planetary Rossby waves. Region of wave breaking in blue oval (near the top of the figure). White arrow is the resulting poleward meridional circulation due to momentum balance.

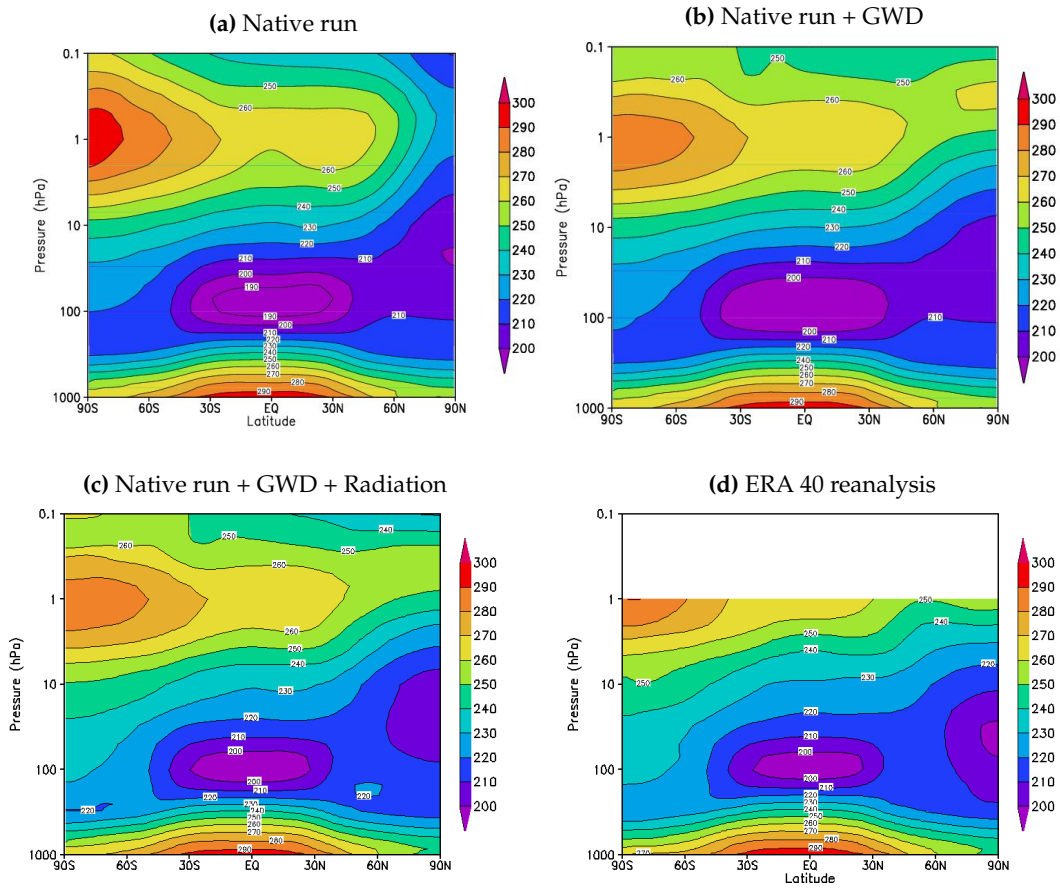


Figure S3. Zonal mean temperature (in $^{\circ}$ K) for Northern hemisphere winter (DJF). (a) GEM-Strato native run 8-year climatology, (b) GEM-Strato with Hines gravity wave drag (15-year climatology), (c) GEM-Strato with Hines gravity wave drag and Li and Barker radiation scheme (15-year climatology), (d) ERA 40 reanalysis

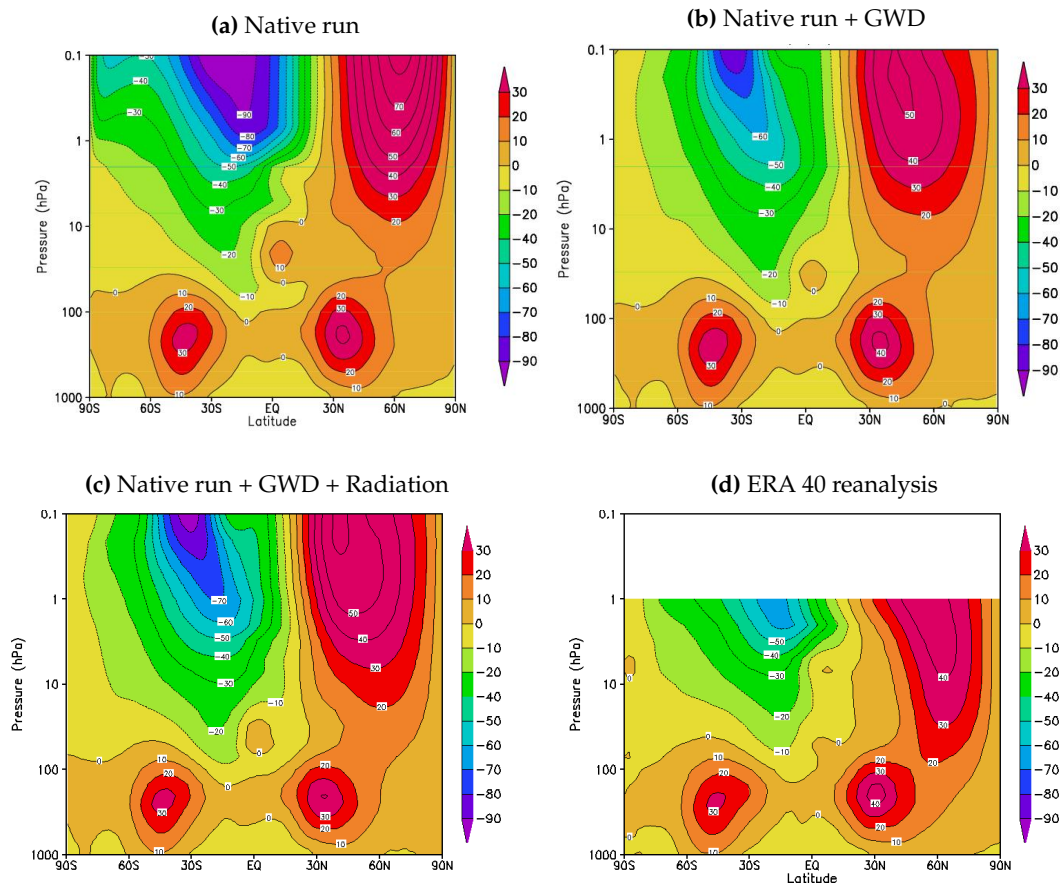


Figure S4. Zonal mean wind (in ms^{-1}) for Northern hemisphere winter (DJF). Panels (a)-(d) same as in Figure S3

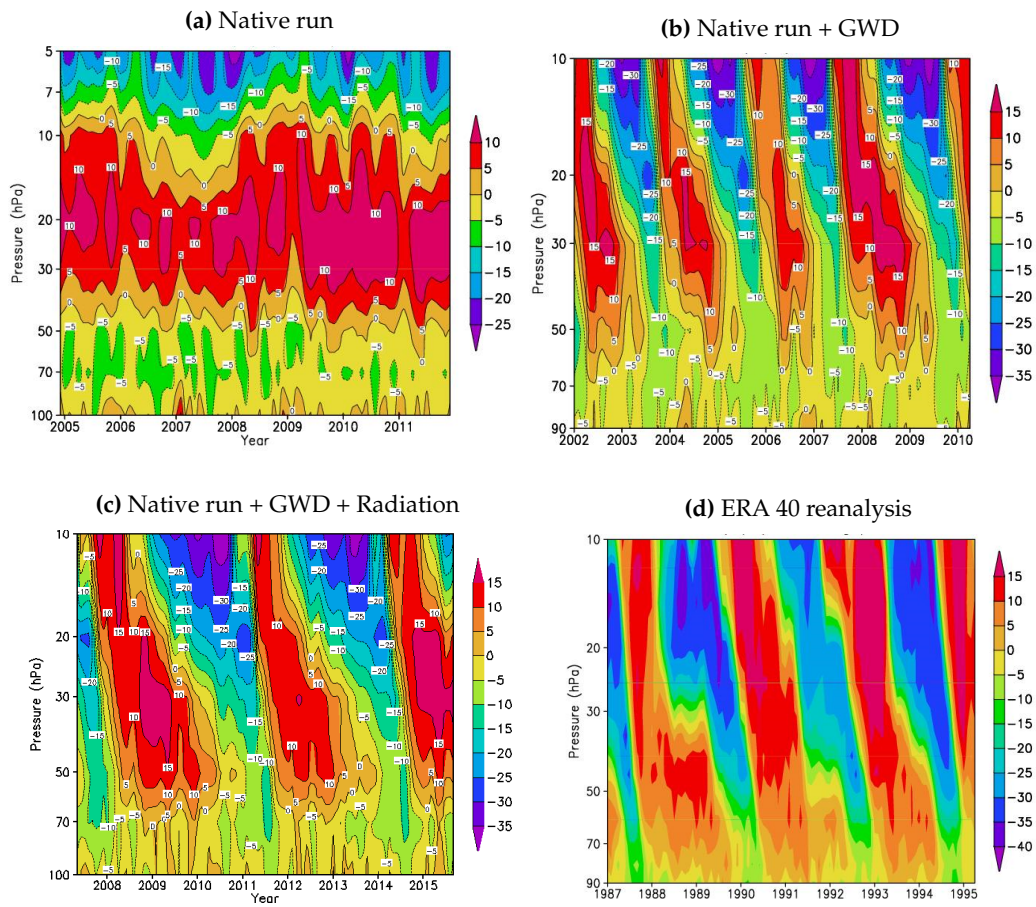


Figure S5. Time series of zonal wind (in ms^{-1}) at the equator. (a) GEM-Strato native run 8-year climatology, (b) GEM-Strato with Hines gravity wave drag (15-year climatology), (c) GEM-Strato with Hines gravity wave drag and Li and Barker radiation scheme (15-year climatology), (d) Zonal wind from the Singapore radiosonde. Note that the years are different in each panel and the vertical scale in panel (a) is slightly different from the other panels.

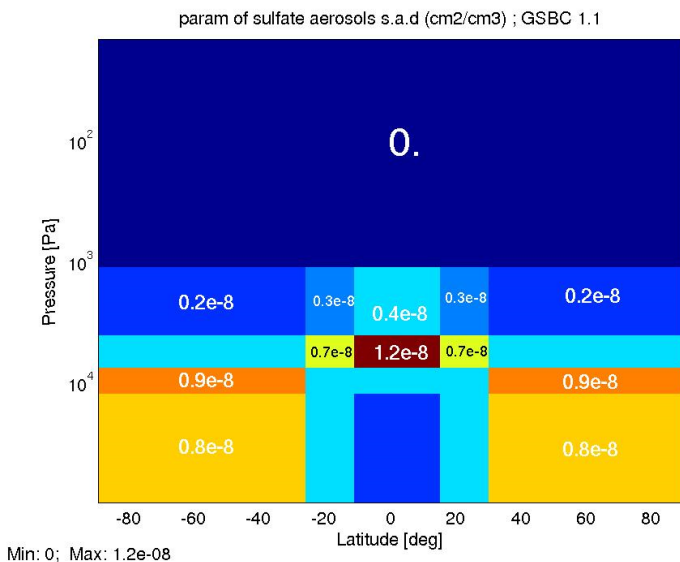


Figure S6. Sulfate aerosols climatology

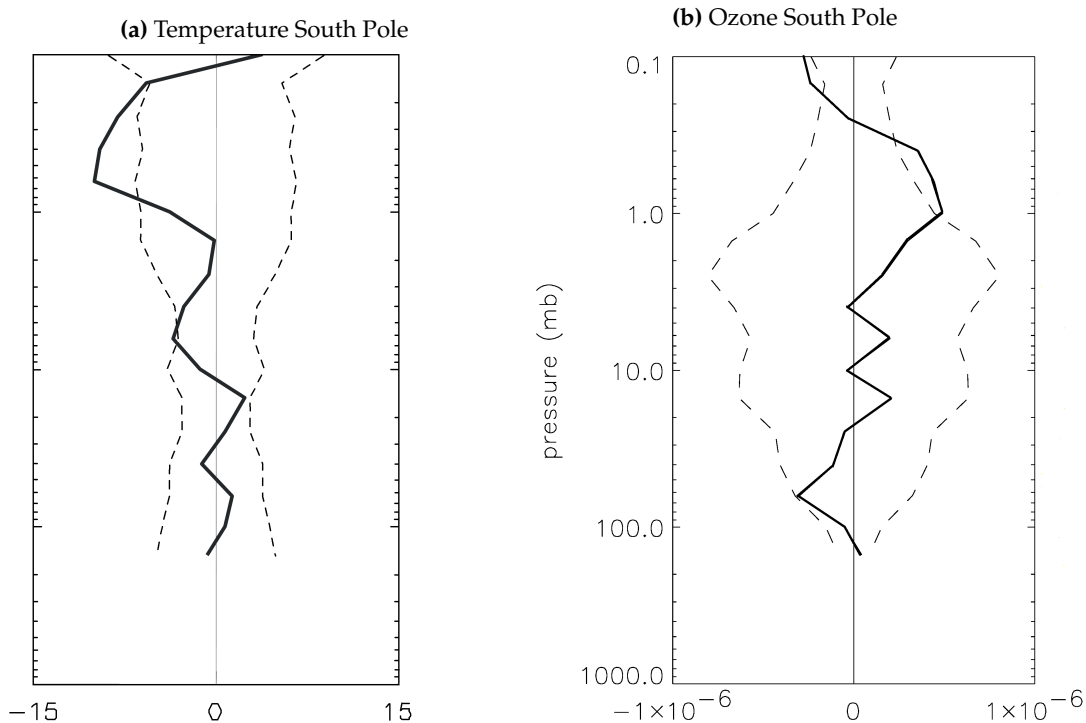


Figure S7. Monthly (August-September 2003) average over the South Pole region (south of 70°S) of MIPAS observations minus GEM-BACH. Left panel shows the difference for temperature in degrees K as a function of height (hPa). Right panel shows the difference for ozone volume mixing ratio. The solid curve is the mean, and the dashed curve is the standard deviation.

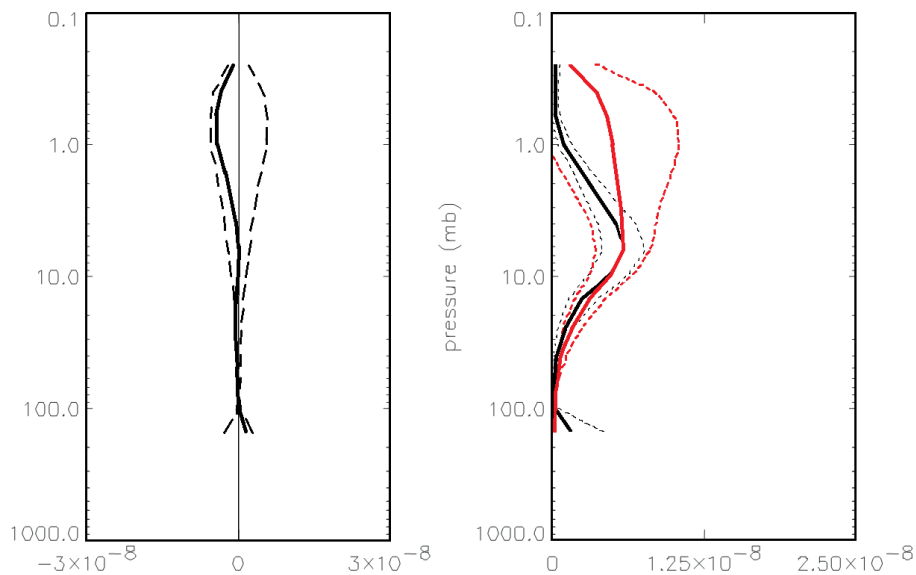


Figure S8. Temporal (August-September 2003) and global average of NO₂ concentration from HALOE and GEM-BACH. Same curve nomenclature as in Figure S7

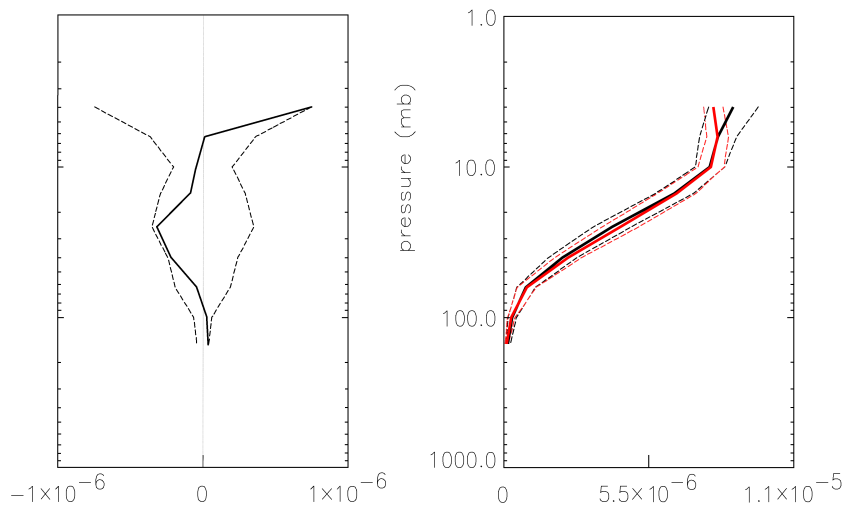


Figure S9. Temporal (August-September 2003) and zonal average of ozone concentrations from sondes and GEM-BACH. The comparison is limited to the 30°N - 50°N latitude band as it contains abundant measurement sites (see Figure S10). Left panel shows the difference between the observation and model in VMR as a function of height (hPa). The solid curve is the mean, and the dashed curve is the standard deviation. Right panel shows the observed profile in black and the GEM-BACH profile in red. Solid line is the mean and the dotted line is the standard deviation.



Figure S10. Spatial distribution of ozone sondes of the WOUDC network

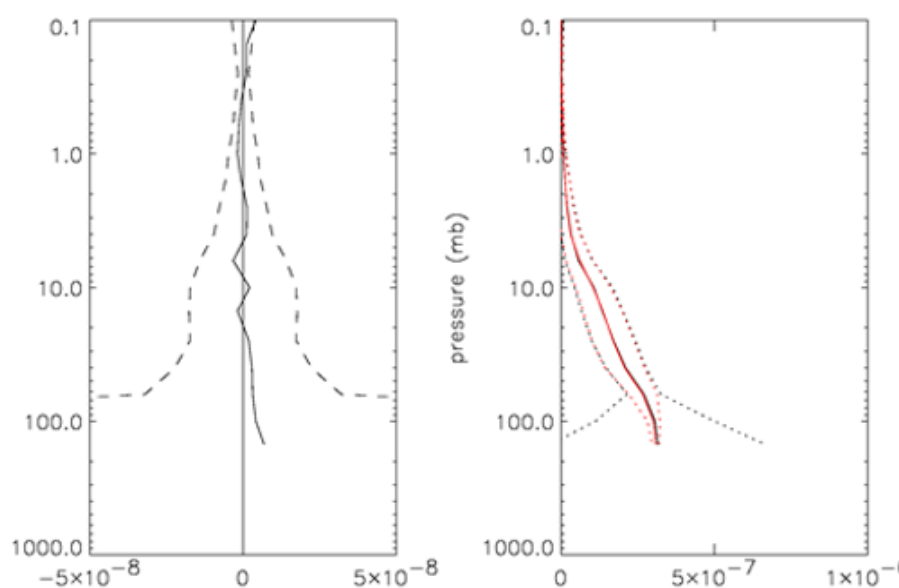


Figure S11. Temporal (August-September 2003) and global average of N_2O concentration from MIPAS and GEM-BACH. Same curve nomenclature as in Figure S9

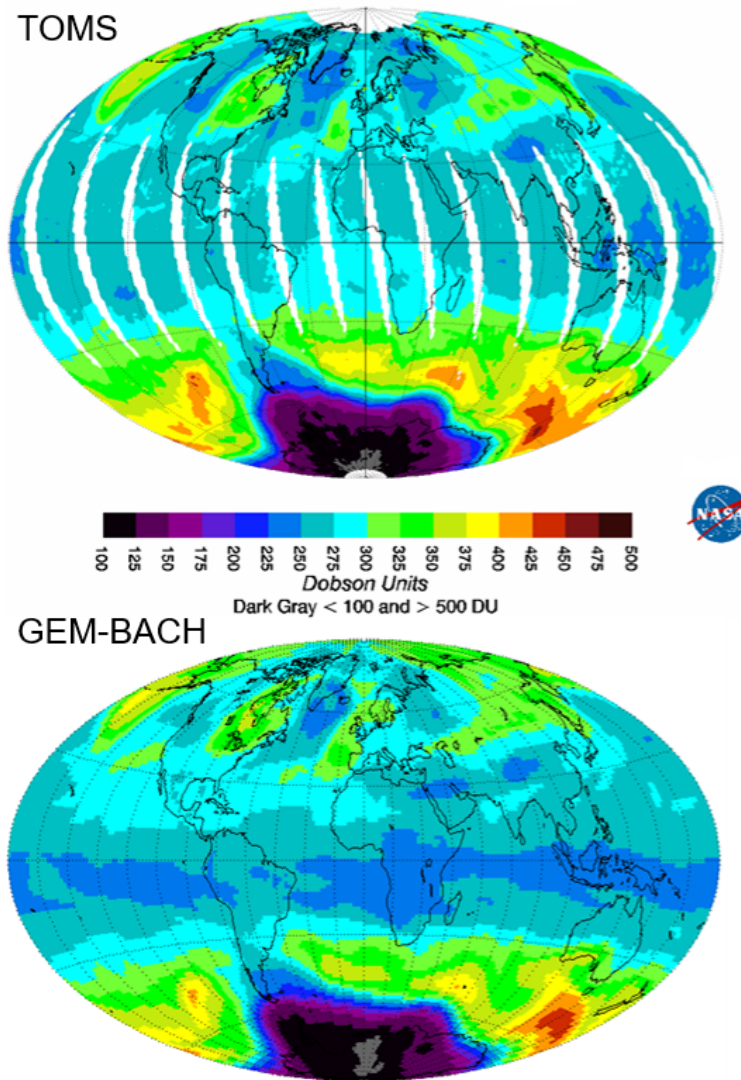


Figure S12. Total column ozone (DU) for September 30th 2003. Upper panel shows mapped TOMS observations (courtesy of NASA Goddard) and lower panel is based on GEM-BACH